Organic Field-Effect Transistors Based on π-Extended Dibenzotetrathiafulvalene Analogues with Thiophene Spacers

Keiko Omata,[1] Masashi Mamada,[1] Jun-ichi Nishida,[1] Shizuo Tokito,[2] and Yoshiro Yamashita*[1]

[1]Department of Electronic Chemistry, Interdisciplinary Graduate School of Science and Engineering, Tokyo Institute of Technology, Nagatsuta, Midori-ku, Yokohama 226-8502

[2]NHK Science and Technical Research Laboratories, Kinuta, Setagaya-ku, Tokyo 157-8510

Received November 4, 2009; E-mail: yoshiro@echem.titech.ac.jp

Dibenzotetrathiafulvalene (DBTTF) analogs containing fused thiophene spacers were synthesized and characterized by cyclic voltammetry, UV–vis absorption spectroscopy, quantum chemical calculations, single-crystal X-ray analysis, overlap integral calculations, field-effect transistor (FET) characteristics, X-ray diffraction, and atomic force microscopy (AFM). The single-crystal X-ray analysis revealed that the DBTTF with a thieno[3,2-*b*]thiophene spacer has a molecular geometry with short intramolecular S···S contacts and a herringbone packing structure with short intermolecular S···S contacts leading to large two-dimensional overlap integrals. The molecule afforded a crystalline thin film with well-ordered molecular orientation corresponding to the single-crystal structure. The FET device based on this molecule exhibited good mobility of 0.29 $cm^2 V^{-1} s^{-1}$ and low threshold voltage of −0.3 V. The effects of the thiophene spacer on the properties, structure, and FET performances were investigated here.

Organic field-effect transistors (OFETs) are of considerable interest due to their potential applications.[1] In OFETs, organic materials such as acenes and oligothiophenes are employed as active layers.[2,3] Tetrathiafulvalene (TTF) derivatives have also been used for OFETs. TTF is a strong electron donor with a low HOMO level and the thin film is easily doped with oxygen or impurities, resulting in unstable FET devices. Introduction of fused aromatic rings to the TTF core is useful to decrease the electron-donating property. In fact, dibenzotetrathiafulvalene (DBTTF, Figure 1) was found to be a good p-type semiconductor for OFETs.[4] On the other hand, π-extended systems have advantages of reduced Coulomb repulsion and enhanced intermolecular interactions.[5] Very recently, OFETs of π-extended DBTTF derivatives with monocyclic aromatic rings such as benzene have been reported.[6] Derivative **1** with a thiophene spacer is also reported there. However, their performances were poorer than that of thin film DBTTF and the effect of π-extension in the spacer has not been investigated. We have now focused on the DBTTF analogs with thiophene spacers because they can be easily prepared and are a hybrid of TTF and thiophene oligomers. The thiophene spacers are expected to tune the properties and structures of TTF. Therefore, in addition to the derivative with a bithiophene spacer **2**, compounds **3** and **4** with fused thiophene rings were used as semiconductors for OFETs because they have more rigid structures and are expected to show stronger intermolecular interactions. We report herein their physical properties, structures, and FET characteristics.

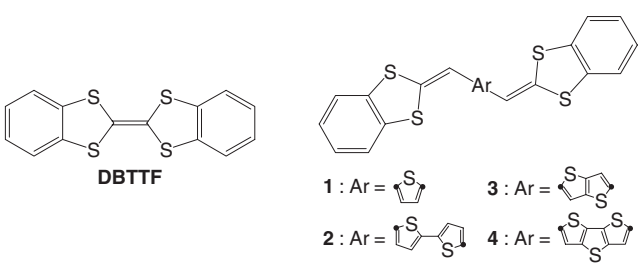

Figure 1. Chamical structures of DBTTF and **1**–**4**.

Experimental

General. Melting points were obtained on a SHIMADZU DSC-60. ^{1}H NMR spectra were recorded on a JEOL JNM-ECP 300 spectrometer and referenced to the residual solvent proton resonance. EI mass spectra were collected on a JEOL JMS-700 mass spectrometer. Elemental analyses were performed at the Tokyo Institute of Technology, Chemical Resources Laboratory. UV–vis spectra were recorded on a SHIMADZU Multi Spec-1500. Cyclic voltammograms were recorded on a HOKUTO DENKO HZ-5000 containing tetrabutylammonium hexafluorophosphate ($TBAPF_6$) (0.1 mol dm^{-3} in dry dichloromethane). A Pt disk, Pt wire, and SCE were used as working, counter, and reference electrodes, respectively. MO calculations were carried out by DFT methods at the B3LYP/6-311G(d)//B3LYP/6-311+G(2d,p) level using the Gaussian program.[7] X-ray diffraction (XRD) measurements were carried out with a JEOL JDX-3530 X-ray diffractometer system. XRD patterns were obtained using Bragg–Brentano geometry with Cu Kα 5 radiation as an X-ray source with an acceleration voltage of 40 kV and a beam current of 30 mA. AFM experiments for films in tapping mode were performed using an SII NanoTechnology SPA-400 (DFM) instrument.

Materials. Triethylamine, THF, and acetonitrile were purchased from Kanto Chemicals. Thiophene was purchased from Acros organics. 2-Bromothiophene and 3-bromothiophene were purchased from Tokyo Kasei Co. These reagents

Published on the web April 29, 2010; doi:10.1246/bcsj.20090290

were used without further purification. 2-Tributylphosphonio-1,3-benzodithiole tetrafluoroborate, thieno[3,2-*b*]thiophene, and dithieno[3,2-*b*;2′,3′-*d*]thiophene were synthesized according to reported methods.[8,9] Bisformylation of thiophene derivatives was carried out by a usual procedure that used *n*-BuLi and DMF.[10]

Synthesis. BT-DBTTF (2): To a solution of [2,2′]bithiophenyl-5,5′-dicarbaldehyde (0.0222 g, 1.00 mmol) in dry THF (100 mL) was added under argon atmosphere 2-tributylphosphonio-1,3-benzodithiole tetrafluoroborate (2.21 g, 5.00 mmol) in dry acetonitrile (20 mL) and triethylamine (10 mL). After stirring for 24 h in the dark at room temperature, the mixture was filtered. The residue was washed with water and methanol, then purified by sublimation to give **2** (0.110 g, 22%) as orange crystals. Mp 311–316 °C. The ^{1}H NMR and ^{13}C NMR could not be taken due to the low solubility. MS/EI (70 eV): *m/z* 494 (M^+, 100%), *m/z* 247 (17.0). Anal. Calcd for $C_{24}H_{14}S_6$: C, 58.26; H, 2.85; S, 38.89%. Found: C, 58.10; H, 2.83; S, 39.12%.

TT-DBTTF (3): Compound **3** was synthesized in 46% yield by a similar method for **2**. Pale brown crystals; mp 372–375 °C. The ^{1}H NMR and ^{13}C NMR could not be taken due to the low solubility. MS/EI (70 eV): *m/z* 468 (M^+, 100%), *m/z* 315 (2.31), *m/z* 283 (3.43), *m/z* 234 (11.9). Anal. Calcd for $C_{22}H_{12}S_6$: C, 56.37; H, 2.58; S, 41.05%. Found: C, 56.13; H, 2.68; S, 41.35%.

DTT-DBTTF (4): Compound **4** was synthesized in 22% yield by a similar method for **2**. Pale orange powder; mp 294–297 °C. The ^{1}H NMR and ^{13}C NMR could not be taken due to the low solubility. MS/EI (70 eV): *m/z* 524 (M^+, 100%), *m/z* 262 (12.8). Anal. Calcd for $C_{24}H_{12}S_7$: C, 54.93; H, 2.30; S, 42.77%. Found: C, 54.76; H, 2.40; S, 42.64%.

X-ray Crystal Structure Analysis. The measurements were carried out on a Rigaku RAXIS-RAPID Imaging Plate diffractometer (Mo Kα radiation, $\lambda = 0.71075$ Å). The data were collected at 93 K and the structures were solved by a direct method (SIR2004[11]) and expanded using Fourier techniques. The non-hydrogen atoms were refined anisotropically. Hydrogen atoms were refined using the riding model.

Crystal Data for 2: $C_{24}H_{14}S_6$, $M_r = 494.73$, crystal dimensions $0.40 \times 0.20 \times 0.01$ mm^3, triclinic, space group $P\bar{1}$, $a = 7.9196(5)$, $b = 9.3265(6)$, $c = 15.2045(9)$ Å, $\alpha = 84.9654(19)$, $\beta = 81.4752(18)$, $\gamma = 66.8480(17)°$, $V = 1020.65(11)$ Å^3, $Z = 2$, $D_{calcd} = 1.610$ g cm^{-3}, 8349 reflections collected, 3740 independent ($R_{int} = 0.037$), GOF = 1.222, $R_1 = 0.0463$, $wR_2 = 0.1362$ for all reflections.

Crystal Data for 3: $C_{22}H_{12}S_6$, $M_r = 468.70$, crystal dimensions $0.10 \times 0.10 \times 0.10$ mm^3, monoclinic, space group $P2_1/n$, $a = 5.8013(8)$, $b = 7.4359(10)$, $c = 43.594(8)$ Å, $\beta = 94.398(6)°$, $V = 1875.0(5)$ Å^3, $Z = 4$, $D_{calcd} = 1.660$ g cm^{-3}, 12412 reflections collected, 4275 independent ($R_{int} = 0.134$), GOF = 1.062, $R_1 = 0.0991$, $wR_2 = 0.2248$ for all reflections.

Crystallographic data have been deposited with Cambridge Crystallographic Data Centre: Deposition number CCDC-734256 for **2** and CCDC-734257 for **3**, respectively. Copies of the data can be obtained free of charge via http://www.ccdc.cam.ac.uk/conts/retrieving.html (or from the Cambridge Crystallographic Data Centre, 12, Union Road, Cambridge, CB2 1EZ, U.K.; Fax: +44 1223 336033; e-mail: deposit@ccdc.cam.ac.uk).

Device Fabrication. The OTS (octyltrichlorosilane) treatment was carried out by immersing the substrate in 0.025 M OTS in toluene at room temperature for 24 h. OFETs were constructed on heavily-doped n-type silicon wafers covered with thermally grown silicon dioxide. The silicon dioxide acts as a gate dielectric layer, and the silicon wafer serves as a gate electrode. Several types of devices which have different configuration, channel length (*L*) and width (*W*) were fabricated.

Bottom contact electrodes: The SiO_2 gate dielectric was 300 nm thick. The source and drain electrodes were Cr (10 nm)/Au (20 nm). L/W was 50/500 μm. Organic semiconductors (500 Å) were deposited on the channel region by vacuum evaporation at a rate of 0.2–0.3 Å s^{-1} under pressure of 10^{-5} Pa. During the evaporation, the temperature of the substrate was maintained at room temperature or 50 °C.

Top contact electrodes: The SiO_2 gate dielectric was 200 nm thick. Organic semiconductors (300 Å) were deposited on the silicon dioxide by vacuum evaporation at a rate of 0.2 Å s^{-1} under pressure of 10^{-5} Pa. Gold was used as source and drain electrodes and deposited on the organic semiconductor layer through a shadow mask with $L/W = 50/1000$ or 50/500 μm.

The FET measurements were carried out at room temperature in a vacuum chamber (10^{-5} Pa) without exposure to air with Hewlett-Packard 4140A and 4140B models.

Mobilities (μ) were calculated in the saturation regime by the relationship: $\mu_{sat} = (2I_D L)/[WC_{ox}(V_G - V_{th})^2]$, where I_D is the source–drain saturation current, C_{ox} (4 F) is the oxide capacitance, V_G is the gate voltage, and V_{th} is the threshold voltage. The latter can be estimated as the intercept of the linear section of the plot of V_G $(I_D)^{1/2}$.

Results and Discussion

Synthesis and Characterization. The synthetic method based on the Wittig reaction is shown in Scheme 1. Although compounds **1** and **2** with thiophene and bithiophene spacers are known,[12] the fused thiophene systems **3** and **4** are new. Thermal properties of these compounds were investigated by differential scanning calorimetry (DSC), which showed only one sharp peak at 248, 314, 373, and 296 °C, respectively. The melting point of **3** is much higher than those of others, suggesting stronger intermolecular interactions in **3**.

Optical and Electrochemical Properties. The data of optical and electrochemical measurements and DFT calculations are summarized in Table 1. The absorption spectra of **1**, **3**, and **4** showed fine structures with two maxima, suggesting

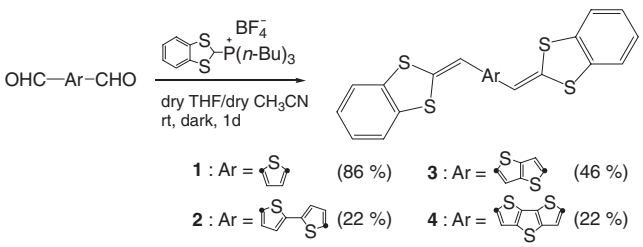

Yields after purification by gradient vacuum sublimation.

Scheme 1. Synthesis of DBTTF derivatives with thiophene spacers.

Table 1. Spectroscopic, Electrochemical, and DFT Caluculation Data

Compd.	Solution					Calculation[d]	
	E_1^{ox}/V	E_2^{ox}/V	λ_{abs}/nm	HOMO[b]	LUMO[c]	HOMO	LUMO
DBTTF	+0.60	+1.01	312	−5.01	−1.76	−5.10	−1.38
1	+0.43	+0.60	419, 441	−4.77	−2.21	−4.73	−1.69
2	+0.52	+0.76	449	−4.86	−2.52	−4.79	−1.98
3	—[a]	—[a]	425, 451	—	—	−4.72	−1.99
4	+0.42	+0.66	436, 464	−4.76	−2.48	−4.76	−1.91

a) Not measured due to low solubility. b) Calculated by oxidation potentials. c) Estimated from $E_{HOMO} = E_{LUMO} - E_{gap}$(optical). d) Based on B3LYP/6-311G(d)//B3LYP/6-311+G(2d,p).

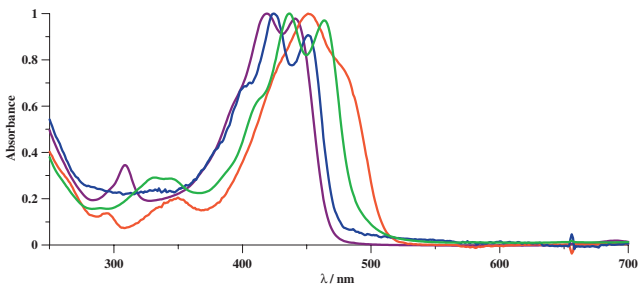

Figure 2. Absorption spectra of **1** (purple line), **2** (orange line), **3** (blue line), and **4** (green line) in dichloromethane solution.

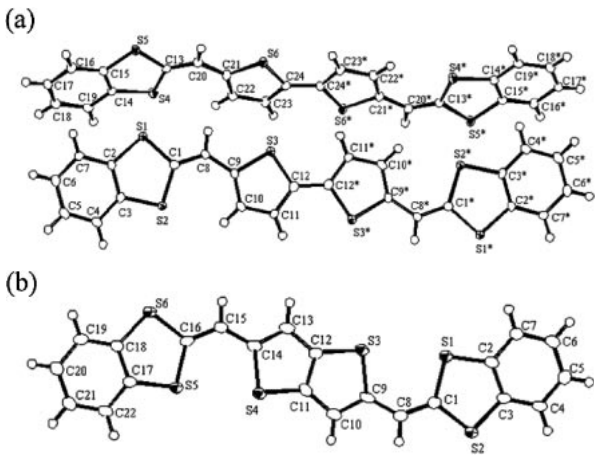

Figure 4. Molecular geometry of (a) **2** and (b) **3**, showing 50% probability displacement ellipsoids.

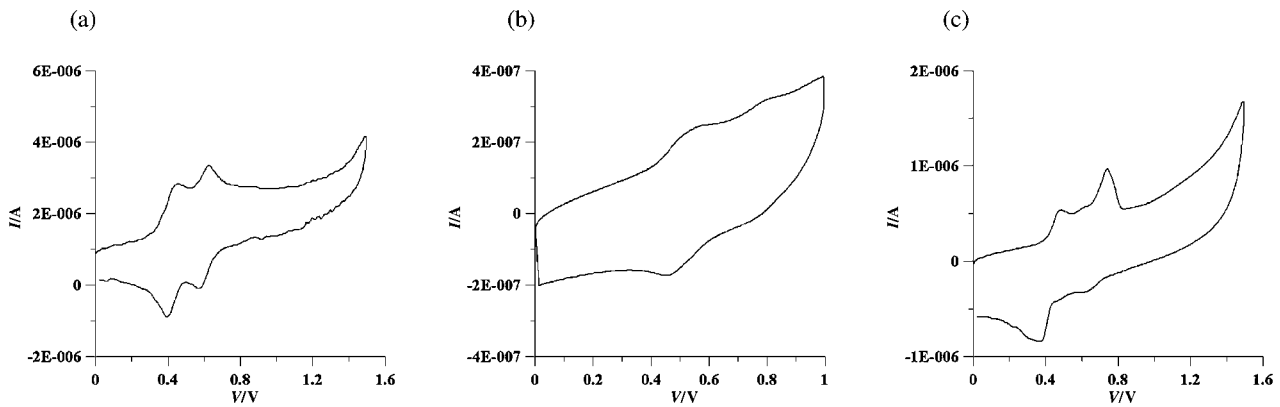

Figure 3. Cyclic voltammograms of (a) **1**, (b) **2**, and (c) **4**.

the rigid structures derived from the fused systems as shown in Figure 2. On the other hand, bithiophene **2** exhibited no vibronic band, suggesting a flexible structure. The extension of π-conjugation leads to bathochromic shifts as found in comparison between **1** and **2** or **3** and **4**. The cyclic voltammograms (CVs) of **1** and **2** exhibited two reversible oxidation peaks associated with generation of cation radicals and dications, whereas the oxidation potentials of **4** are complicated due to the oxidation of the fused thiophene unit as shown in Figure 3. The CV of **3** could not be measured due to the low solubility. The first oxidation potentials of π-extended systems are negatively shifted compared to that of DBTTF, indicating the higher HOMO levels. Bithiophene **2** showed slightly higher oxidation potentials than **1**. The differences between the first and second oxidation potentials of π-extended systems are smaller than that of DBTTF due to reduction of Coulombic repulsion. The HOMO energies estimated from the first oxidation potentials are ca. 4.8 eV, which are consistent with the values obtained by DFT calculations.

X-ray Single Crystal Analysis. The single crystals of **2** and **3** were obtained by slow sublimation although those of **1** and **4** could not be obtained. Figure 4 shows the molecular geometry of **2** and **3** obtained by X-ray structure analysis. The crystal of **2** has two crystallographically independent molecules in the unit cell. The two molecules are almost planar and the dihedral angles between the benzo-1,3-dithiole and thiophene

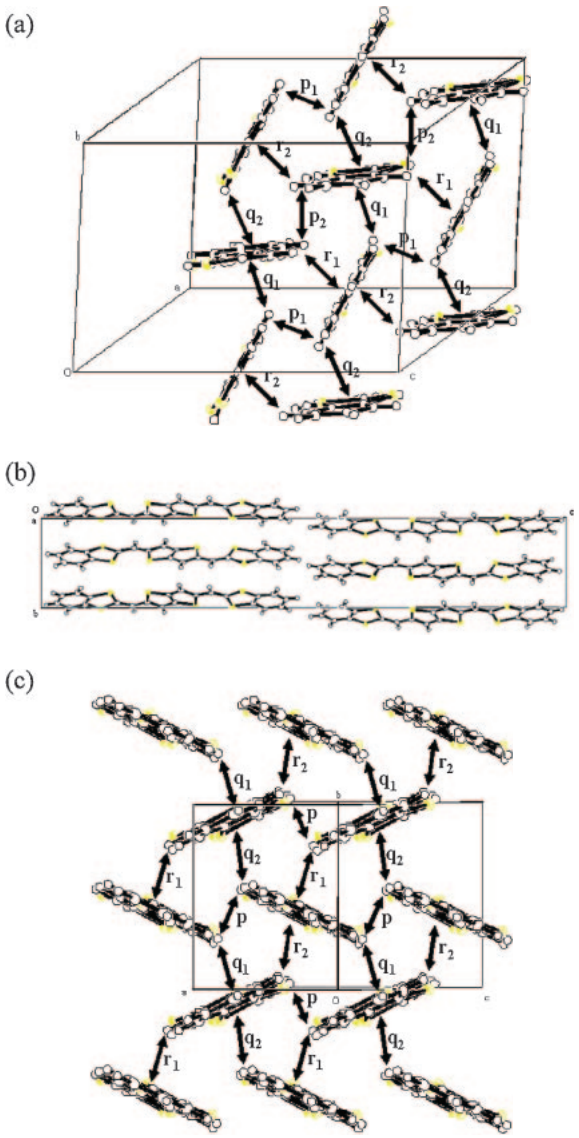

Figure 5. (a) The packing structure in **2** viewing from the long molecular axis. (b) The packing structure of **3** along the *a* axis. (c) The packing structure in **3** viewing from the long molecular axis.

rings are 1.4–7.5°. The molecule of **3** is also nearly planar and the dihedral angles between the benzo-1,3-dithiole and thienothiophene rings are 7.8–11.3°. Interestingly, the direction of the 1,3-dithiole rings toward the thiophene rings is different between **2** and **3**. Thus, molecules of **2** have a geometry with no S···S contacts, where the sulfur atoms of thiophenes are far from the 1,3-dithiole rings. In contrast, the sulfur atoms of the thienothiophene ring in **3** face the 1,3-dithiole rings, where S···S contacts of ca. 3.1 Å are observed. Figure 5 shows the packing structures of **2** and **3**, both of which are a herringbone type with a tilt angle of 51.5 and 48.0°, respectively. The molecular long axis of **3** is perpendicular to the *ab* plane in the unit cell. The crystal of **2** showed no S···S intermolecular interactions, whereas **3** has intermolecular S···S short contacts of ca. 3.3 Å, suggesting the presence of strong intermolecular interactions in **3**.

Table 2. FET Characteristics of **1**–**4** Devices Fabricated on OTS-Treated Substrates with Bottom Contact Configuration[a)]

Compd.	T_{sub} /°C	Mobility /cm^2 V^{-1} s^{-1}	On/off ratio	Threshold /V
1	rt	0.097	3×10^3	−1.6
	50	0.038	1×10^4	−0.3
2	rt	0.078	1×10^4	−4.3
3	rt	0.23	6×10^4	−5.4
	50	0.29	1×10^3	−0.3
4	rt	0.029	7×10^3	−14

a) SiO_2: 300 nm, $L/W = 50/500$ µm, S/D electrodes: Cr(10 nm)/Au(20 nm).

Table 3. FET Characteristics of **1**, **2**, and **3** Devices Fabricated on OTS-Treated Substrates with Top Contact Configuration[a)]

Compd.	T_{sub} /°C	Mobility /cm^2 V^{-1} s^{-1}	On/off ratio	Threshold /V
1	rt	0.015	1×10^5	−10
2	rt	0.033	2×10^5	−8.2
3	rt	0.12	7×10^5	−10
4	rt	no gate effect		

a) SiO_2: 200 nm, $L/W = 50/1000$ µm, S/D electrodes: Au(50 nm).

Overlap Integral Calculations. The overlap integrals "*S*" between the molecules were calculated from the HOMOs using the extended Hückel method based on the molecular geometry obtained by the X-ray single crystal structures.[13] The overlap integrals of **2** were $S_{p1} = 7.3 \times 10^{-4}$, $S_{p2} = 7.5 \times 10^{-4}$, $S_{q1} = 1.9 \times 10^{-3}$, $S_{q2} = 1.9 \times 10^{-3}$, $S_{r1} = 5.2 \times 10^{-4}$, $S_{r2} = 5.2 \times 10^{-4}$. Those of **3** were $S_p = 1.5 \times 10^{-3}$, $S_{q1} = 1.8 \times 10^{-3}$, $S_{q2} = 1.3 \times 10^{-3}$, $S_{r1} = 1.8 \times 10^{-3}$, $S_{r2} = 1.3 \times 10^{-3}$. The S_p in **3** is much larger than those in **2**, resulting in two-dimensional overlap. This is attributed to the intermolecular S···S contacts in **3**. For comparison, the overlap integrals of DBTTF were calculated (see Supporting Information). There are polymorphic forms in the single crystals of DBTTF.[14] The single crystal called α phase shows a high mobility of 1 cm^2 V^{-1} s^{-1} in a single-crystal FET device. Its overlap integrals were calculated to be $S_p = 5.4 \times 10^{-3}$ and $S_q = 9.8 \times 10^{-6}$, where the π-stack direction S_p is much larger than the side direction S_q. This result suggests that **3** has a larger two-dimensional nature than the α phase of DBTTF crystal. The β phase of DBTTF with a herringbone packing showed 7.1×10^{-4} to 7.0×10^{-5} of overlap integrals by calculations, which are smaller than those of **3**.

OFET Characteristics. The FET devices were fabricated by vacuum deposition. The FET characteristics are summarized in Table 2 (bottom contact) and Table 3 (top contact). These devices showed typical p-channel characteristics (Figure 6) and no hysteresis behavior. The device characteristics of bottom contact devices were slightly better than those of top contact ones. The top contact device of **4** did not show FET characteristics. The mobilities of these devices were from 10^{-2} to 10^{-1} cm^2 V^{-1} s^{-1} and the threshold voltages were very low. Among those materials, the thienothiophene derivatives **3**

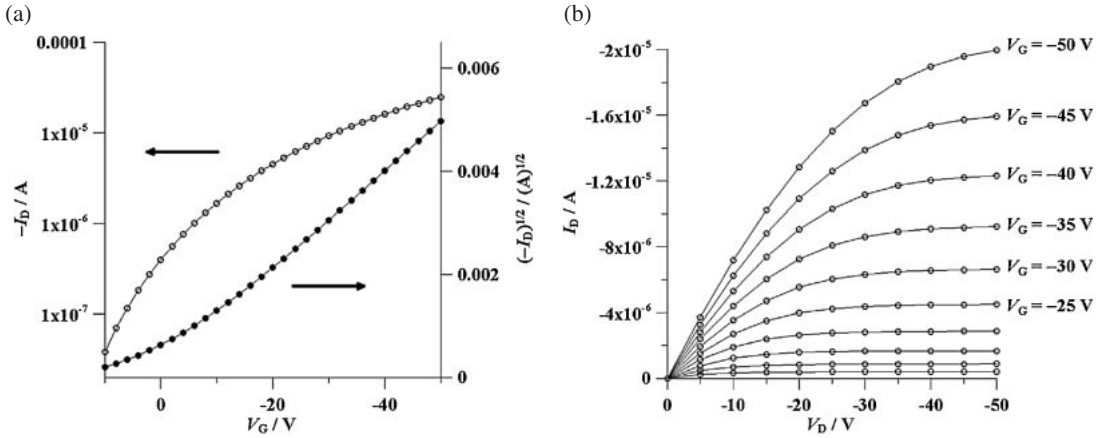

Figure 6. (a) Drain current (I_D) and ($I_D^{1/2}$) versus gate voltage at drain voltage (V_D) of −50 V transfer characteristics for **3** on the OTS-treated substrate (T_{sub} = 50 °C). (b) I_D versus V_D output characteristics for **3** on the OTS-treated substrate (T_{sub} = 50 °C).

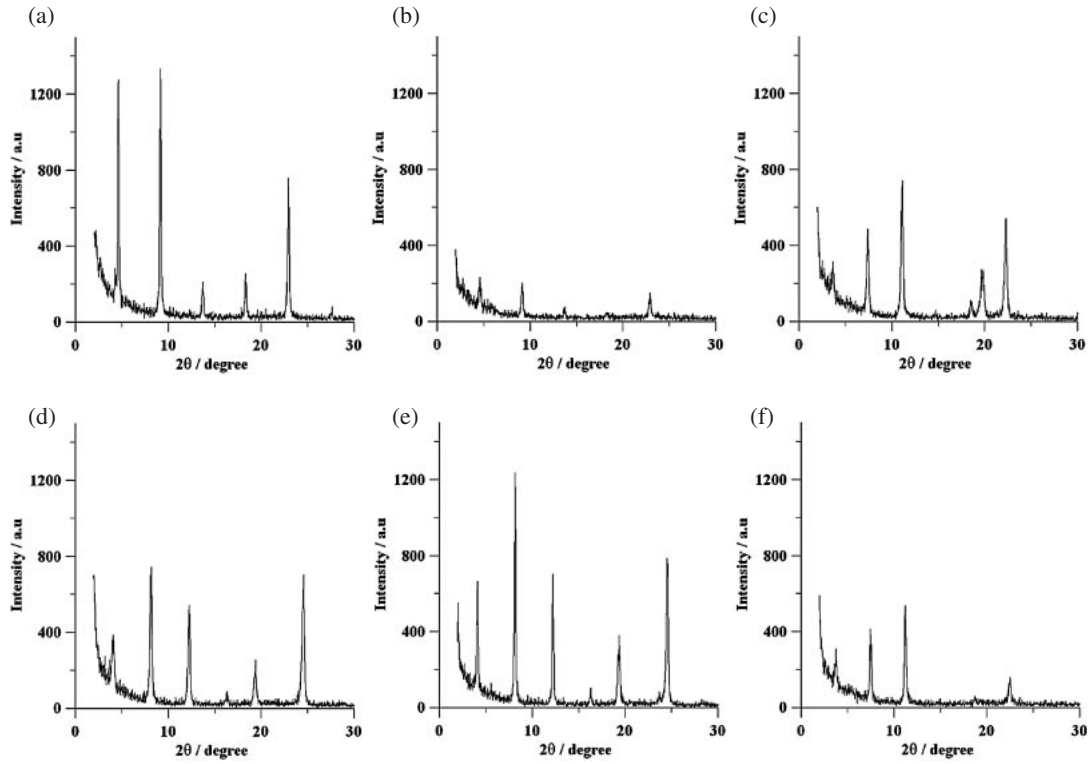

Figure 7. X-ray diffractograms of 50 nm films deposited on the OTS-treated substrate at (a) rt for **1**, (b) 50 °C for **1**, (c) rt for **2**, (d) rt for **3**, (e) 50 °C for **3**, and (f) rt for **4**.

exhibited the best performance with good mobility of 0.23 $cm^2 V^{-1} s^{-1}$, high on/off ratio of 6×10^4 and low threshold voltage of −5.4 V. The mobility of thin film DBTTF under the same conditions was 0.08 $cm^2 V^{-1} s^{-1}$, and the optimized value was 0.19 $cm^2 V^{-1} s^{-1}$,[4e] indicating that the mobility of **3** is higher than that of DBTTF. This is attributed to the large two-dimensional intermolecular interactions including S···S interactions in **3** as found in the calculations of transfer integrals. The mobility of **3** was improved by increasing the substrate temperature to 0.29 $cm^2 V^{-1} s^{-1}$. In contrast, the device of **1** fabricated at higher substrate temperatures showed lower mobility. These results indicate that the FET performances of DBTTF analogs are strongly dependent on the thiophene spacer. All of the bottom contact devices based on these compounds showed FET behavior only for short times in air. The mobilities in air were the same or slightly higher compared with those in vacuum conditions. The on/off ratios decreased due to the oxygen doping, resulting in increase of the off current.[15] In addition, a positive shift of threshold voltage, which often happens with oxygen doping, was also observed. Although the devices of **2**, **3**, and **4** did not work as FET after 24 h in air, the device of **1** showed the FET performance for a few days in air.

X-ray Diffractogram. Figure 7 shows X-ray diffractograms (XRD) of the thin films of **1**–**4**. The reflections up to high orders were observed in all of the films deposited at room

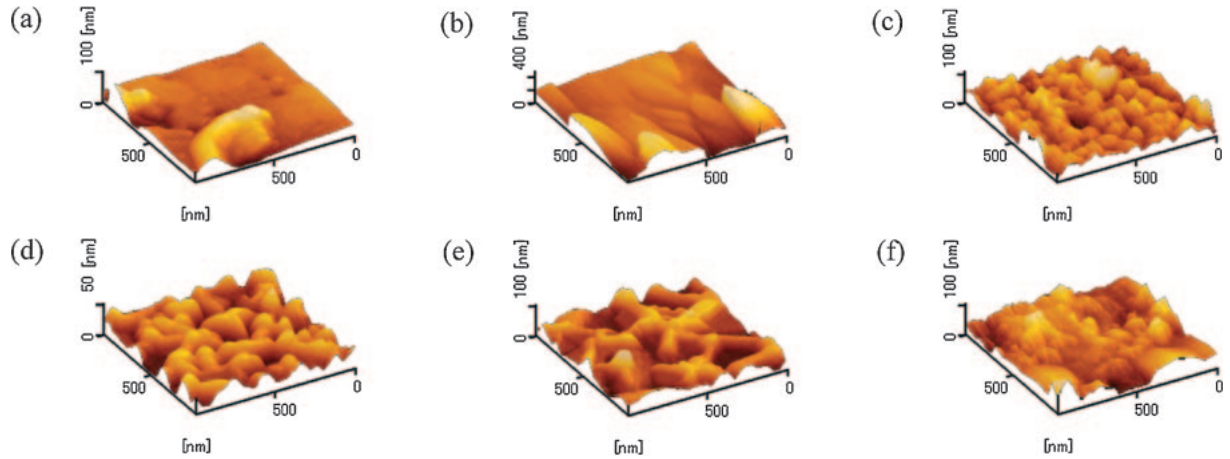

Figure 8. AFM images of thin film deposited on OTS-treated substrate at (a) rt for **1**, (b) 50 °C for **1**, (c) rt for **2**, (d) rt for **3**, (e) 50 °C for **3**, and (f) rt for **4**.

temperature, indicating formation of lamellar ordering and crystallinity on the substrate. The film of **3** deposited at 50 °C (Figure 7e) showed sharper reflection peaks, whereas the film of **1** deposited at 50 °C (Figure 7b) showed very weak peaks. This amorphous-like morphology is considered to cause the poorer FET characteristics of **1** film deposited at 50 °C. The *d*-spacing of thin film **3** obtained from the first reflection peak ($2\theta = 4.06$) is 21.7 Å, which is identical to the simulation pattern (002) obtained from the single crystal data. Since the long axis of molecule is in the direction of *c* axis (43.54 Å) of the unit cell as shown in Figure 5b, molecule **3** is considered to be perpendicular on the substrate. On the other hand, the *d*-spacing of thin film **2** is 23.7 Å, which is almost the same as the molecular length (23.0 Å), indicating the perpendicular molecular orientation. However, the crystal structure does not correspond to the molecular orientation, suggesting that the film structure is different from the crystal structure. The *d*-spacing of thin film **1** (19.3 Å) and **4** (23.6 Å) suggests their linear molecular geometry with no S···S contacts between the 1,3-dithioles and thiophene sulfur atoms. It is different from the structures expected from the single crystal structure of a TTF analog with a thiophene spacer, which exhibits intramolecular S···S contacts.[12c,16]

AFM Measurements. Figure 8 shows the tapping mode atomic force microscopy (AFM) images of the thin films of **1**–**4**. The surface of the thin film of **1** is relatively flat, though a large grain can be seen partially. As the substrate temperature is increased, the surface becomes a granular structure and the flatness is decreased, but the grain boundary is still not observed. The absence of grain boundary seems related to the air stability in **1** because oxygen invasion is suppressed in no grain structure. On the other hand, the thin film of **2** shows a number of small uniform grains even at room temperature. Similarly, many small grains can be observed in the thin film of **3**. The grain becomes larger and continuous at 50 °C. This result supports the higher performance of **3** deposited at 50 °C. The thin film of **4** is composed of a mixture of small and large grains, and the surface is significantly rough. This morphology is believed to prevent the contact between the electrodes and the semiconductor in the top contact device, resulting in no field-effect characteristics.

Conclusion

We have developed a series of DBTTF analogs with thiophene spacers for OFETs, and their solid-state structures and thin film characteristics were characterized. The molecular geometry and OFET characteristics were strongly dependent on the spacers. In the single crystal, the DBTTF analog with a thieno[3,2-*b*]thiophene spacer has a molecular geometry with short intramolecular S···S contacts between the 1,3-dithiole and thiophene rings and short intermolecular S···S contacts are also observed. On the other hand, the bithiophene derivative has neither intra- nor intermolecular S···S contacts in the crystal. The OFET based on the thienothiophene derivative showed a mobility of $0.29\,cm^2\,V^{-1}\,s^{-1}$, which is higher than those of DBTTF and the derivative with a bithiophene spacer. This is attributed to the large two-dimensional overlap of molecular orbitals and highly ordered lamellar structure in the thin film of the thienothiophene derivative. This result suggests that the π-extended TTF analogs with two-dimensional intermolecular interactions are promising semiconductors for high-performance OFETs.

This work is supported by a Grant-in-Aid for Scientific Research (No. 19350092) from the Ministry of Education, Culture, Sports, Science and Technology, Japan, and Mizuho Foundation for the Promotion of Sciences, the Global COE program "Education and Research Center for Emergence of New Molecular Chemistry" and the Research Fellow of the Japan Society for the Promotion of Science.

Supporting Information

Differential pulse voltammograms, UV–vis absorption spectra, DFT calculations, single crystal structures, overlap integral calculations, AFM measurements, and FET characteristics. These materials are available free of charge on the web at http://www.csj.jp/journals/bcsj/.

References

1 a) H. E. Katz, *Chem. Mater.* **2004**, *16*, 4748. b) M. Muccini, *Nat. Mater.* **2006**, *5*, 605. c) L. Zhou, A. Wanga, S.-C. Wu, J. Sun,

S. Park, T. N. Jackson, *Appl. Phys. Lett.* **2006**, *88*, 083502. d) J. Zaumseil, H. Sirringhaus, *Chem. Rev.* **2007**, *107*, 1296. e) M. Berggren, D. Nilsson, N. D. Robinson, *Nat. Mater.* **2007**, *6*, 3.

2 a) T. W. Kelley, D. V. Muyres, P. F. Baude, T. P. Smith, T. D. Jones, *Mater. Res. Soc. Symp. Proc.* **2003**, *771*, 169. b) C. D. Sheraw, T. N. Jackson, D. L. Eaton, J. E. Anthony, *Adv. Mater.* **2003**, *15*, 2009. c) M. M. Payne, S. R. Parkin, J. E. Anthony, C.-C. Kuo, T. N. Jackson, *J. Am. Chem. Soc.* **2005**, *127*, 4986. d) H. Meng, F. Sun, M. B. Goldfinger, F. Gao, D. J. Londono, W. J. Marshal, G. S. Blackman, K. D. Dobbs, D. E. Keys, *J. Am. Chem. Soc.* **2006**, *128*, 9304. e) T. Yamamoto, K. Takimiya, *J. Am. Chem. Soc.* **2007**, *129*, 2224. f) M. L. Tang, A. D. Reichardt, N. Miyaki, R. M. Stoltenberg, Z. Bao, *J. Am. Chem. Soc.* **2008**, *130*, 6064.

3 a) G. Horowitz, F. Garnier, A. Yassar, R. Hajlaoui, F. Kouki, *Adv. Mater.* **1996**, *8*, 52. b) M. Halik, H. Klauk, U. Zschieschang, G. Schmid, W. Radlik, S. Ponomarenko, S. Kirchmeyer, W. Weber, *J. Appl. Phys.* **2003**, *93*, 2977. c) M. Halik, H. Klauk, U. Zschieschang, G. Schmid, S. Ponomarenko, S. Kirchmeyer, W. Weber, *Adv. Mater.* **2003**, *15*, 917. d) A. Facchetti, M. Mushrush, M. H. Yoon, G. R. Hutchison, M. A. Ratner, T. J. Marks, *J. Am. Chem. Soc.* **2004**, *126*, 13859.

4 a) M. Mas-Torrent, P. Hadley, S. T. Bromley, N. Crivillers, J. Veciana, C. Rovira, *Appl. Phys. Lett.* **2005**, *86*, 012110. b) Naraso, J. Nishida, S. Ando, J. Yamaguchi, K. Itaka, H. Koinuma, H. Tada, S. Tokito, Y. Yamashita, *J. Am. Chem. Soc.* **2005**, *127*, 10142. c) Y. Takahashi, T. Hasegawa, Y. Abe, Y. Tokura, K. Nishimura, G. Saito, *Appl. Phys. Lett.* **2005**, *86*, 063504. d) Y. Takahashi, T. Hasegawa, Y. Abe, Y. Tokura, G. Saito, *Appl. Phys. Lett.* **2006**, *88*, 073504. e) K. Shibata, K. Ishikawa, H. Takezoe, H. Wada, T. Mori, *Appl. Phys. Lett.* **2008**, *92*, 023305. f) T. Yoshino, K. Shibata, H. Wada, Y. Bando, K. Ishikawa, H. Takezoe, T. Mori, *Chem. Lett.* **2009**, *38*, 200.

5 M. Takada, H. Graaf, Y. Yamashita, H. Tada, *Jpn. J. Appl. Phys.* **2002**, *41*, L4.

6 O. Alévêque, P. Frère, P. Leriche, T. Breton, A. Cravino, J. Roncali, *J. Mater. Chem.* **2009**, *19*, 3648.

7 M. J. Frisch, G. W. Trucks, H. B. Schlegel, G. E. Scuseria, M. A. Robb, J. R. Cheeseman, J. A. Montgomery, Jr., T. Vreven, K. N. Kudin, J. C. Burant, J. M. Millam, S. S. Iyengar, J. Tomasi, V. Barone, B. Mennucci, M. Cossi, G. Scalmani, N. Rega, G. A. Petersson, H. Nakatsuji, M. Hada, M. Ehara, K. Toyota, R. Fukuda, J. Hasegawa, M. Ishida, T. Nakajima, Y. Honda, O. Kitao, H. Nakai, M. Klene, X. Li, J. E. Knox, H. P. Hratchian, J. B. Cross, V. Bakken, C. Adamo, J. Jaramillo, R. Gomperts, R. E. Stratmann, O. Yazyev, A. J. Austin, R. Cammi, C. Pomelli, J. W. Ochterski, P. Y. Ayala, K. Morokuma, G. A. Voth, P. Salvador, J. J. Dannenberg, V. G. Zakrzewski, S. Dapprich, A. D. Daniels, M. C. Strain, O. Farkas, D. K. Malick, A. D. Rabuck, K. Raghavachari, J. B. Foresman, J. V. Ortiz, Q. Cui, A. G. Baboul, S. Clifford, J. Cioslowski, B. B. Stefanov, G. Liu, A. Liashenko, P. Piskorz, I. Komaromi, R. L. Martin, D. J. Fox, T. Keith, M. A. Al-Laham, C. Y. Peng, A. Nanayakkara, M. Challacombe, P. M. W. Gill, B. Johnson, W. Chen, M. W. Wong, C. Gonzalez, J. A. Pople, *Gaussian 03, Revision C.02*, Gaussian, Inc., Wallingford CT, **2004**.

8 a) J. Nakayama, *Synthesis* **1975**, 38. b) J. Nakayama, K. Fujiwara, M. Hoshino, *Bull. Chem. Soc. Jpn.* **1976**, *49*, 3567. c) K. Akiba, K. Ishikawa, N. Inamoto, *Bull. Chem. Soc. Jpn.* **1978**, *51*, 2674.

9 a) Y. Mazaki, K. Kobayashi, *Tetrahedron Lett.* **1989**, *30*, 3315. b) F. Allared, J. Hellberg, T. Remonen, *Tetrahedron Lett.* **2002**, *43*, 1553.

10 P. Leriche, J.-M. Raimundo, M. Turbiez, V. Monroche, M. Allain, F.-X. Sauvage, J. Roncali, P. Frère, P. J. Skabara, *J. Mater. Chem.* **2003**, *13*, 1324.

11 SIR2004: M. C. Burla, R. Caliandro, M. Camalli, B. Carrozzini, G. L. Cascarano, L. De Caro, C. Giacovazzo, G. Polidori, R. J. Spagna, *J. Appl. Crystallogr.* **2005**, *38*, 381.

12 a) A. S. Benahmed-Gasmi, P. Frère, B. Garrigues, A. Gorgues, M. Jubault, R. Carlier, F. Texier, *Tetrahedron Lett.* **1992**, *33*, 6457. b) A. S. Benahmed-Gasmi, P. Frère, M. Jubault, A. Gorgues, J. Cousseau, B. Garrigues, *Synth. Met.* **1993**, *56*, 1751. c) J. Roncali, L. Rasmussen, C. Thobie-Gautier, P. Frère, H. Brisset, M. Sallé, J. Becher, O. Simonsen, T. K. Hansen, A. Benahmed-Gasmi, J. Orduna, J. Garin, M. Jubault, A. Gorgues, *Adv. Mater.* **1994**, *6*, 841. d) A. Benahmed-Gasmi, P. Frère, J. Roncali, E. Elandaloussi, J. Orduna, J. Garin, M. Jubault, A. Gorgues, *Tetrahedron Lett.* **1995**, *36*, 2983. e) J. Roncali, *J. Mater. Chem.* **1997**, *7*, 2307.

13 T. Mori, A. Kobayashi, Y. Sasaki, H. Kobayashi, G. Saito, H. Inokuchi, *Bull. Chem. Soc. Jpn.* **1984**, *57*, 627.

14 a) T. J. Emge, F. M. Wiygul, J. S. Chappell, A. N. Bloch, J. P. Ferraris, D. O. Cowan, T. J. Kistenmacher, *Mol. Cryst. Liq. Cryst.* **1982**, *87*, 137. b) A. Brillante, I. Bilotti, R. G. D. Valle, E. Venuti, S. Milita, C. Dionigi, F. Borgatti, A. N. Lazar, F. Biscarini, M. Mas-Torrent, N. S. Oxtoby, N. Crivillers, J. Veciana, C. Rovira, M. Leufgen, G. Schmidt, L. W. Molenkamp, *CrystEngComm* **2008**, *10*, 1899.

15 a) R. Ye, M. Baba, K. Suzuki, Y. Ohishi, K. Mori, *Thin Solid Films* **2004**, *464–465*, 437. b) D. Kumaki, M. Yahiro, Y. Inoue, S. Tokito, *Appl. Phys. Lett.* **2007**, *90*, 133511.

16 a) J. Roncali, L. Rasmussen, C. Thobie-Gautier, P. Frère, H. Brisset, M. Sallé, J. Becher, O. Simonsen, T. K. Hansen, A. Benahmed-Gasmi, J. Orduna, J. Garin, M. Jubault, A. Gorgues, *Adv. Mater.* **1994**, *6*, 841. b) P. Frère, P. J. Skabara, *Chem. Soc. Rev.* **2005**, *34*, 69.